Geophysical Research Letters

RESEARCH LETTER
10.1029/2022GL098506

Seasonal Landslide Activity Lags Annual Precipitation Pattern in the Pacific Northwest

L. V. Luna[1,2,3] **and O. Korup**[1,2]

[1]Institute of Environmental Science and Geography, University of Potsdam, Potsdam, Germany, [2]Institute of Geosciences, University of Potsdam, Potsdam, Germany, [3]Potsdam Institute for Climate Impact Research, Potsdam, Germany

Key Points:

- Bayesian inference learns the seasonal pattern of landslide activity in the Pacific Northwest from five combined heterogeneous inventories
- Landsliding is distinctly seasonal with highest probability (intensity) in January (February), lagging the annual precipitation peak
- Landslide intensity for a given monthly rainfall during peak season in February is up to 10 times higher than at the onset in November

Supporting Information:

Supporting Information may be found in the online version of this article.

Correspondence to:

L. V. Luna,
luna@uni-potsdam.de

Citation:

Luna, L. V., & Korup, O. (2022). Seasonal landslide activity lags annual precipitation pattern in the Pacific Northwest. *Geophysical Research Letters*, *49*, e2022GL098506. https://doi.org/10.1029/2022GL098506

Received 28 FEB 2022
Accepted 15 SEP 2022

Abstract Seasonal variations in landslide activity remain understudied compared to recent advances in landslide early warning at hourly to daily timescales. Here, we learn the seasonal pattern of monthly landslide activity in the Pacific Northwest from five heterogeneous landslide inventories with differing spatial and temporal coverage and reporting protocols combined in a Bayesian multi-level model. We find that landslide activity is distinctly seasonal, with credible increases in landslide intensity, inter-annual variability, and probability marking the onset of the landslide season in November. Peaks in landslide probability in January and intensity in February lag the annual peak in mean monthly precipitation and landslide activity is more variable in winter than in summer, when landslides are rare. For a given monthly rainfall, landslide intensity at the season peak in February is up to 10 times higher than at the onset in November, underlining the importance of antecedent seasonal hillslope conditions.

Plain Language Summary Better knowing when landslides are likely over the course of the year can reduce landslide risk by improving emergency preparedness. One research challenge is that catalogs of past landslides rarely cover the same areas or time periods, and have been collected in different ways. Here, we use statistical models to estimate monthly landslide activity in the Pacific Northwest. The models are able to combine five different landslide catalogs to make best use of all available information. We find a seasonal pattern in both the average number of landslides in a month and the probability of having any landslides. The landslide season begins in November, when the average number and the probability of landslides increase. The probability of landslides peaks in January and the average number in February, lagging behind winter rainfall peaks by one to two months. While landslides are least likely in summer, their activity is more variable in winter, with some winters bringing hundreds of landslides, and some very few. At the landslide season peak in February, a comparable amount of rain leads to many more landslides than at the onset in November, likely because already wet hillslopes are more prone to failure.

1. Introduction

Landslides regularly cause fatalities and damage infrastructure in many areas worldwide (Froude & Petley, 2018), and extensive research has focused on anticipating *where* landslides are likely to occur (Reichenbach et al., 2018). For people living in susceptible areas, however, better constraining *when* landslides are likely is key to reducing risk, as taking proper action can increase survival rates (Pollock & Wartman, 2020). Globally, advances in landslide early warning have mostly concentrated on hourly to daily timescales (Baum & Godt, 2010; Guzzetti et al., 2020; Mirus, Becker, et al., 2018; Stanley et al., 2021). Much less attention has been given to quantifying seasonal patterns of landslide activity, which would allow for improved planning and emergency preparedness to be able to quickly react to short-term warnings.

To characterize landslide seasonality, previous studies have, for example, modeled monthly rock fall frequency along a rail corridor in British Columbia (Pratt et al., 2019), investigated seasonal trends in modeled daily landslide hazard in the Pacific Northwest (PNW) of the United States (Stanley et al., 2020), or explored seasonal changes in intensity-duration thresholds for rainfall-triggered landslides in Italy (Napolitano et al., 2016; Nikolopoulos et al., 2015; Peruccacci et al., 2012). Other authors have connected increased landslide activity with seasonal changes in precipitation and hillslope hydrologic conditions, especially during the wetter winter season in the PNW (Godt et al., 2006; Mirus, Morphew, & Smith, 2018). Studies reporting a seasonal distribution of landslides often rely on two metrics: the number (or frequency) of landslides and the presence or absence of landslides (Saito et al., 2010; Schneuwly-Bollschweiler & Stoffel, 2012; Sepúlveda & Petley, 2015).

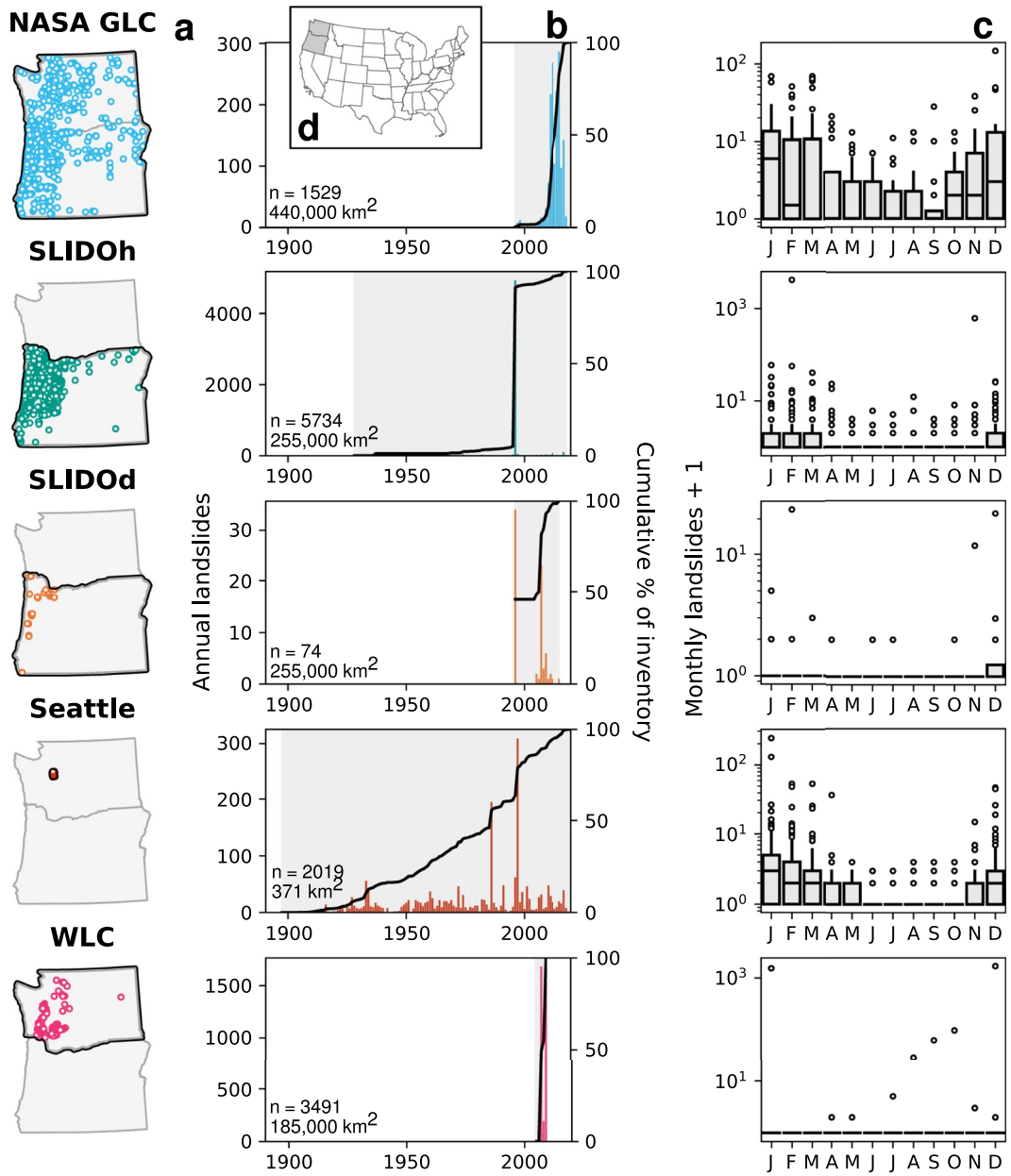

Figure 1. Reported landslides in the Pacific Northwest from five inventories. (a) Locations of landslides with monthly time-stamps (open circles) and footprint area covered by each inventory (black outline) in Washington and Oregon (b). (c) Annual time series of landslides (colored bars) over the period of record (gray shading). Black line indicates cumulative proportion of landslides recorded over time. (d) Box plots show the distribution of landslides in each month (box encloses the interquartile range, horizontal line is the median, whiskers cover 1.5 times the interquartile range); "+1" allows for display of months with no landslides on a log-scale.

Here, our objectives are to (a) test with statistical models whether these two descriptive metrics objectively reveal seasonal variations in landslide activity in the PNW and (b) test if landslide response to precipitation changes seasonally. We use Bayesian inference to estimate monthly landslide intensity and probability from five different landslide inventories from the region (Figure 1 and Table S1 in Supporting Information S1), employing one set of models that learn from landslide inventories alone and another that is conditioned on monthly precipitation over the inventory areas. Using Bayesian models in landslide research (Berti et al., 2012; Korup, 2021; Lombardo et al., 2020; Nolde & Joe, 2013) has the advantage of providing intrinsic and objective estimates of parameter uncertainty, a metric too often neglected in landslide studies (Segoni et al., 2018).

Yet, a challenge in modeling landslide activity is that different inventories report landslides in various ways, and with differing spatial and temporal coverage (Steger et al., 2017). In the PNW, a number of inventories capture quite diverse aspects of landsliding (Figure 1 and Table S1 in Supporting Information S1). The NASA Global Landslide Catalog (NASA GLC), for example, largely relied on news and highway department reports, documenting landslides along roads and in urban areas (Kirschbaum et al., 2015; NASA, 2018). The Washington Landslide Compilation (WLC), on the other hand, mapped widespread shallow landsliding events from LiDAR, aerial photographs, and field visits (Washington Geological Survey, 2020). Bayesian multi-level regression makes use of the combined diverse, if not seemingly incompatible, information on landslide timing contained in these heterogeneous inventories, while still providing estimates for each inventory individually. Our results provide quantitative expectations for monthly landslide probability, intensity, and inter-annual variability in the PNW, inclusive of all uncertainty learned from the data.

2. Study Area and Data

The PNW has one of the highest concentrations of mapped landslides in the United States (Mirus et al., 2020). We focused on the states of Washington and Oregon (Figure 1d), which are topographically characterized by two mountain ranges, a lower coastal range and the higher Cascades Range, to the east of which relief is generally lower. Precipitation in the region has a strong west to east gradient controlled to first order by orographic effects. Mean annual precipitation to the west of the Cascades ranges from ∼1,000 to >4,000 mm and drops to <500 mm to the east (PRISM Climate Group, 2021).

We analyzed five landslide inventories that cover parts or all of Washington and Oregon and include information on landslide timing (Figure 1 and Table S1 in Supporting Information S1). Mapped landslide concentration is highest in and to the west of the Cascades, and the length of record varies from 6 to 122 years between inventories (Figure 1). We considered only those landslides with at least a known month of occurrence, which represent <1–100% of each inventory (Table S1 in Supporting Information S1). Where recorded, most landslides were categorized as rainfall-triggered shallow landslides or debris flows. Depending on the inventory, landslides were mapped through field, LiDAR, or imagery analysis, or collected from news articles, highway reports, consulting reports or other records (Table S1 in Supporting Information S1).

We subset the NASA GLC to Washington and Oregon (NASA, 2018). We treated the Statewide Landslide Information Database for Oregon (SLIDO) historical points data set (SLIDOh) and the landslide polygons data set (SLIDOd) separately, as they resulted from different reporting protocols (Franczyk et al., 2020). We also included all landslides with monthly time-stamps from the Seattle Historic Landslide Locations (Seattle) (City of Seattle, 2020) and WLC (Washington Geological Survey, 2020) inventories, with the exception of the 1980 eruption of Mt. St. Helens.

We used two 4-km resolution precipitation datasets over the inventory areas: the PRISM 30-year Normals (Norm91m) describes average monthly precipitation (Ppt) between 1991 and 2020, while PRISM AN81m provides monthly estimates of precipitation (PRISM Climate Group, 2021). For consistency with the normals data, we analyzed all years between 1991 and 2020 in the AN81m data, computing the spatial mean of both datasets across each inventory footprint area (Figure 1).

3. Methods

We trained two variants of Bayesian multi-level regression models to learn the seasonal pattern of landslide activity at monthly resolution. We used negative binomial regression to estimate the number of landslides reported in a given month (intensity) and logistic regression to estimate the presence or absence of reported landslides (probability). For each regression, we first fit models to inventory data alone to obtain the seasonal landslide pattern without any other predictors (landslide-only models). We then included spatially averaged monthly precipitation per inventory area (1991–2020) as a predictor in these generalized linear models to test for a seasonal landslide response to precipitation (landslide-precipitation models).

We chose Bayesian multi-level models because they are able to share information between landslide inventories, taking advantage of the diverse information contained in the different inventories (multi-inventory models). At the same time, the models provide parameter estimates for each inventory individually, thus respecting some of the important differences between inventories, like the area covered. In these models, the landslide data are grouped by month of occurrence and by inventory, hence one set of parameters is learned for each month and inventory. These parameter estimates are informed by a higher-level distribution of (hyper-)parameters that is also learned from the data and acts as an adaptive prior for each individual month and inventory. In this

way, information is shared across inventories, which has a regularizing effect and generally improves estimates for groups with few observations while preventing overfitting to groups with many observations (Gelman & Hill, 2007; McElreath, 2020). For comparison, we also fit the landslide-only models to each inventory separately (single-inventory models). By binning our data into monthly intervals, we acknowledge the lack of any finer, for example, daily, resolution that would require regression models with autocorrelation terms.

We fit the landslide-only negative binomial models to the number of landslides (y_i) that occurred in each month m recorded in each inventory v. For each month and inventory, the model learned a mean ($\mu_{m,v}$) intensity or expected number of landslides per area, and a shape parameter ($\phi_{m,v}$). The negative binomial distribution's variance is a function of μ and ϕ and represents the inter-annual variability in the number of monthly landslides. In the five single-inventory models, the data were grouped by month and in the multi-inventory model, the data were grouped by month and inventory (Equation 1).

$$\begin{aligned} y_{i,m,v} &\sim \text{Negative Binomial } (\mu_{m,v}, \phi_{m,v}) \\ \ln(\mu_{m,v}) &= (\beta_0 + \beta_{0,m} + \beta_{0,v}) + \ln(A_v) \\ \ln(\phi_{m,v}) &= \gamma_0 + \gamma_{0,m} + \gamma_{0,v} \\ \beta_{0,m} &\sim \text{Normal } (0, \sigma_{0,m}) \\ \beta_{0,v} &\sim \text{Normal } (0, \sigma_{0,v}) \\ \gamma_{0,m} &\sim \text{Normal } (0, \psi_m) \\ \gamma_{0,v} &\sim \text{Normal } (0, \psi_v) \end{aligned} \tag{1}$$

where β_0 and γ_0 are population-level intercepts, $\beta_{0,m}$ and $\gamma_{0,m}$ are group-level intercepts for month, and $\beta_{0,v}$ and $\gamma_{0,v}$ are group-level intercepts for inventory (which are excluded in the single-inventory models). A_v is the footprint area of the inventory. The distribution of the group-level intercepts, which serve as adaptive priors for each individual group-level intercept, are specified as normal distributions with zero means and standard deviations $\sigma_{0,m}$ and ψ_m, and $\sigma_{0,v}$ and ψ_v. Prior distributions must be defined for β_0, γ_0, $\sigma_{0,m}$, ψ_m, $\sigma_{0,v}$, and ψ_v. For all models, we used weakly informative Student's t priors that are implemented as widely applicable defaults in the R package brms, which we used to fit the models (Bürkner, 2017).

The landslide-precipitation negative binomial models follow the same structure, but include precipitation as a predictor.

$$\begin{aligned} y_{i,m,v} &\sim \text{Negative Binomial } (\mu_{i,m,v}, \phi_{m,v}) \\ \ln(\mu_{m,v}) &= (\beta_0 + \beta_{0,m} + \beta_{0,v}) + (\beta_1 + \beta_{1,m} + \beta_{1,v})\, P_{i,m,v} + \ln(A_v) \\ \ln(\phi_{m,v}) &= \gamma_0 + \gamma_{0,m} + \gamma_{0,v} \\ \begin{bmatrix} \beta_{0,m} \\ \beta_{1,m} \end{bmatrix} &\sim MV\,\text{Normal}\left(\begin{bmatrix} 0 \\ 0 \end{bmatrix}, \begin{bmatrix} \sigma_{0,m}^2 & \sigma_{0,m}\sigma_{1,m}\rho_m \\ \sigma_{0,m}\sigma_{1,m}\rho_m & \sigma_{1,m}^2 \end{bmatrix} \right) \\ \begin{bmatrix} \beta_{0,v} \\ \beta_{1,v} \end{bmatrix} &\sim MV\,\text{Normal}\left(\begin{bmatrix} 0 \\ 0 \end{bmatrix}, \begin{bmatrix} \sigma_{0,v}^2 & \sigma_{0,v}\sigma_{1,v}\rho_v \\ \sigma_{0,v}\sigma_{1,v}\rho_v & \sigma_{1,v}^2 \end{bmatrix} \right) \\ \gamma_{0,m} &\sim \text{Normal } (0, \psi_m) \\ \gamma_{0,v} &\sim \text{Normal } (0, \psi_v) \end{aligned} \tag{2}$$

where β_1 is the population-level coefficient of precipitation, $\beta_{1,m}$ and $\beta_{1,v}$ are group-level coefficients with corresponding group-level standard deviations $\sigma_{1,m}$ and $\sigma_{1,v}$, and $P_{i,m,v}$ is the spatially averaged precipitation over the inventory area for a specific month between 1991 and 2020, standardized to the mean precipitation across all inventories and all months. The correlations ρ_m and ρ_v between group-level intercepts and coefficients of precipitation are also learned. We chose a uniform prior for β_1 and a non-informative Cholesky LKJ prior for the correlation matrix (Lewandowski et al., 2009; Stan Development Team, 2022).

Besides estimating the number of landslides, we also used logistic regression to model the presence or absence of reported landslides. Logistic regression relies on a Bernoulli likelihood with parameter $p_{m,v}$ expressing the probability of having at least one landslide reported in a given month. We fit the logistic regression to data that indicate whether one or more landslides were recorded in an inventory in a given month (z_i). Again, we fit a model to data from each inventory and a model to data from all inventories for the landslide-only models (Equation 3).

$$\begin{aligned} z_{i,m,v} &\sim \text{Bernoulli}\ (p_{m,v}) \\ \text{logit}\,(p_{m,v}) &= \alpha_0 + \alpha_{0,m} + \alpha_{0,v} \\ \alpha_{0,m} &\sim \text{Normal}\ (0, \tau_{0,m}) \\ \alpha_{0,v} &\sim \text{Normal}\ (0, \tau_{0,v}) \end{aligned} \tag{3}$$

where $p_{m,v}$ is a function of a population-level intercept α_0 and group-level intercepts $\alpha_{0,m}$ for months and $\alpha_{0,v}$ for inventories (excluded from the single-inventory models), and $\tau_{0,m}$ and $\tau_{0,v}$ are the standard deviations of the group-level intercepts.

The landslide-precipitation logistic regression models again include standardized precipitation as a predictor:

$$\begin{aligned} z_{i,m,v} &\sim \text{Bernoulli}\ (p_{i,m,v}) \\ \text{logit}\ (p_{i,m,v}) &= (\alpha_0 + \alpha_{0,m} + \alpha_{0,v}) + (\alpha_1 + \alpha_{1,m} + \alpha_{1,v})\, P_{i,m,v} \\ \begin{bmatrix} \alpha_{0,m} \\ \alpha_{1,m} \end{bmatrix} &\sim MV\ \text{Normal}\left(\begin{bmatrix} 0 \\ 0 \end{bmatrix}, \begin{bmatrix} \tau_{0,m}^2 & \tau_{0,m}\tau_{1,m}\upsilon_m \\ \tau_{0,m}\tau_{1,m}\upsilon_m & \tau_{1,m}^2 \end{bmatrix} \right) \\ \begin{bmatrix} \alpha_{0,v} \\ \alpha_{1,v} \end{bmatrix} &\sim MV\ \text{Normal}\left(\begin{bmatrix} 0 \\ 0 \end{bmatrix}, \begin{bmatrix} \tau_{0,v}^2 & \tau_{0,v}\tau_{1,v}\upsilon_v \\ \tau_{0,v}\tau_{1,v}\upsilon_v & \tau_{1,v}^2 \end{bmatrix} \right) \end{aligned} \tag{4}$$

where α_1 is the population-level coefficient of precipitation, and $\alpha_{1,m}$ and $\alpha_{1,v}$ are group-level coefficients for months and inventories with corresponding standard deviations $\tau_{1,m}$ and $\tau_{1,v}$. υ_m and υ_v are the correlations between group-level intercepts and coefficients of precipitation.

We fit all models with the R package brms version 2.17.0 (Bürkner, 2017). Brms calls Stan, a probabilistic programming language that uses Hamiltonian Monte Carlo to approximate the posterior parameter space (Stan Development Team, 2022). We ran the sampler for 2,000 iterations for four independent chains, discarding the first 500 draws as warm up, and checked that the chains converged. The single-inventory negative binomial model for WLC did not converge, likely because nearly all landslides recorded in this inventory happened in 2 months; we excluded this model from further analysis.

The model results are posterior parameter estimates conditional on the landslide inventory data, and, for the landslide-precipitation models, monthly precipitation (Figures 2, 3, and Figures S1–S4 in Supporting Information S1). We defined parameter estimates to be credibly distinguishable, for example, between subsequent months, if their 95% highest-density-intervals (HDIs) did not overlap. Finally, we integrated over the posterior parameter estimates to characterize the distribution of landslide activity, thus naturally propagating all uncertainties in our summarized simulated landslide counts and presences/absences (Figure 2). These are called posterior predictive distributions in Bayesian statistics. We also report posterior expectations across all precipitation values for November and February for the landslide-precipitation models (Figure 3).

4. Results

Both our landslide-only multi-inventory models confirm a distinct seasonal pattern of landslide activity in the PNW (Figure 2). Expected monthly landslide intensity is highest in January and February, decreases from March to May, and is lowest in June (dark green points in Figure 2a). Posterior estimates remain low from July to October, before increasing in November and December. This trend is consistent across all inventories, despite differences in reporting protocols and sample size. We can credibly distinguish (95% HDI) mean landslide intensity between subsequent months from February to April and from October to November in the NASA, Seattle, and SLIDOh inventories (Figure 2a). Landslide intensities per unit area are highest in the Seattle inventory and lowest in SLIDOd, with January landslide intensities in Seattle exceeding those in SLIDOd by more than

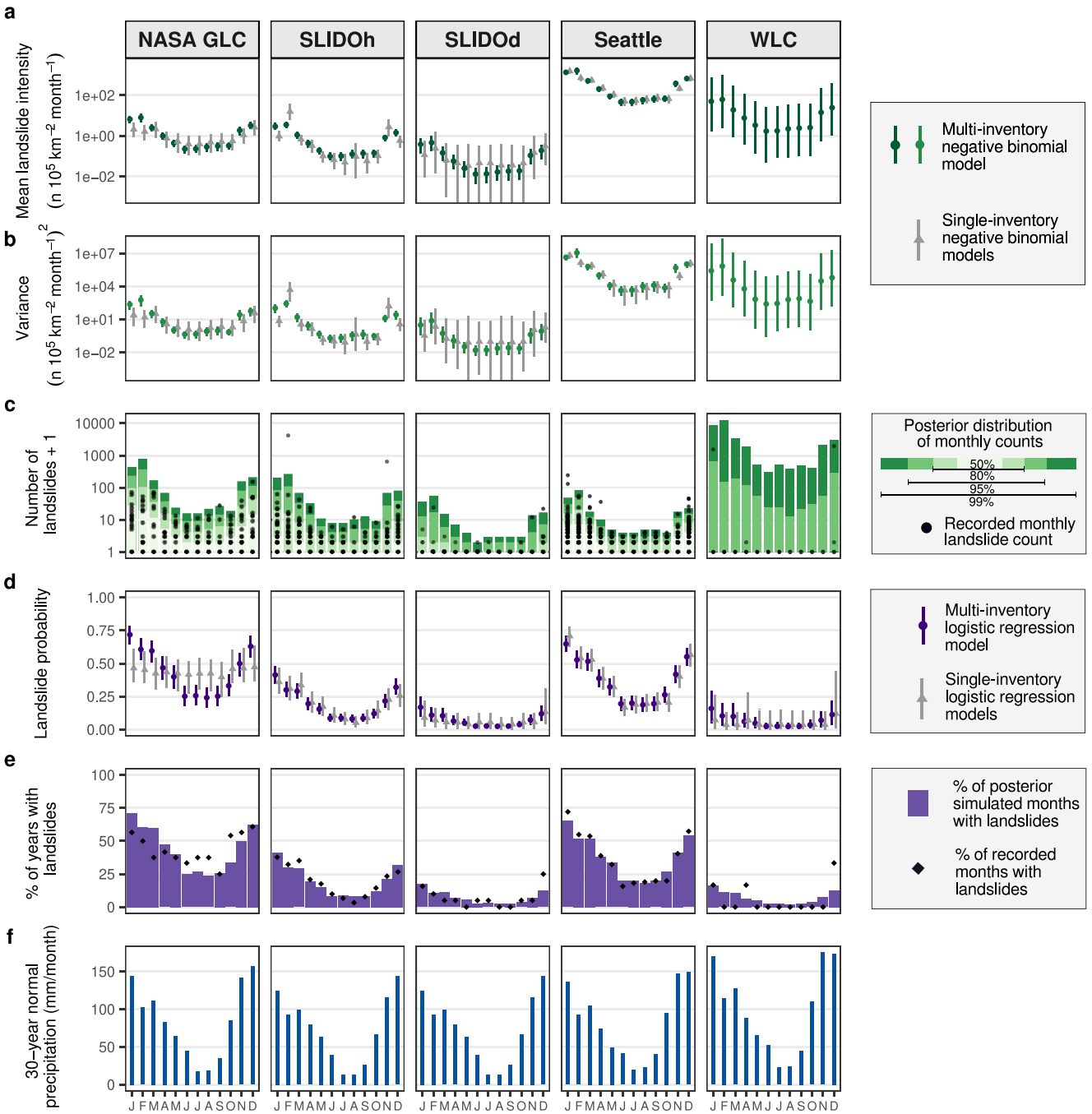

Figure 2. (a–e) Seasonal pattern of landslide activity from inventory-only models compared to (f) 30-year normal monthly precipitation. (a) Posterior parameter estimates for mean monthly landslide intensity, (b) variance, and (d) probability (median and 95% highest-density-interval [HDI]). Two months are considered credibly different when their 95% HDIs do not overlap. (c) Distribution of posterior simulated counts and (e) months with landslides from the multi-inventory models. (f) Mean monthly precipitation over the inventory areas from 1991 to 2020 PRISM climate normals (PRISM Climate Group, 2021).

three orders of magnitude. Monthly variance is also seasonal: highest from November to February and lowest from May through October (Figure 2b). The amplitude of the seasonal intensity pattern in a given inventory is smaller than between inventories (Figure 2a and Figure S1 in Supporting Information S1). Simulated posterior distributions of landslide counts are consistent with the data. Depending on the inventory, the model estimates up to tens to thousands of landslides in winter with 1% posterior probability, whereas median estimates range from zero to two landslides (Figure 2c).

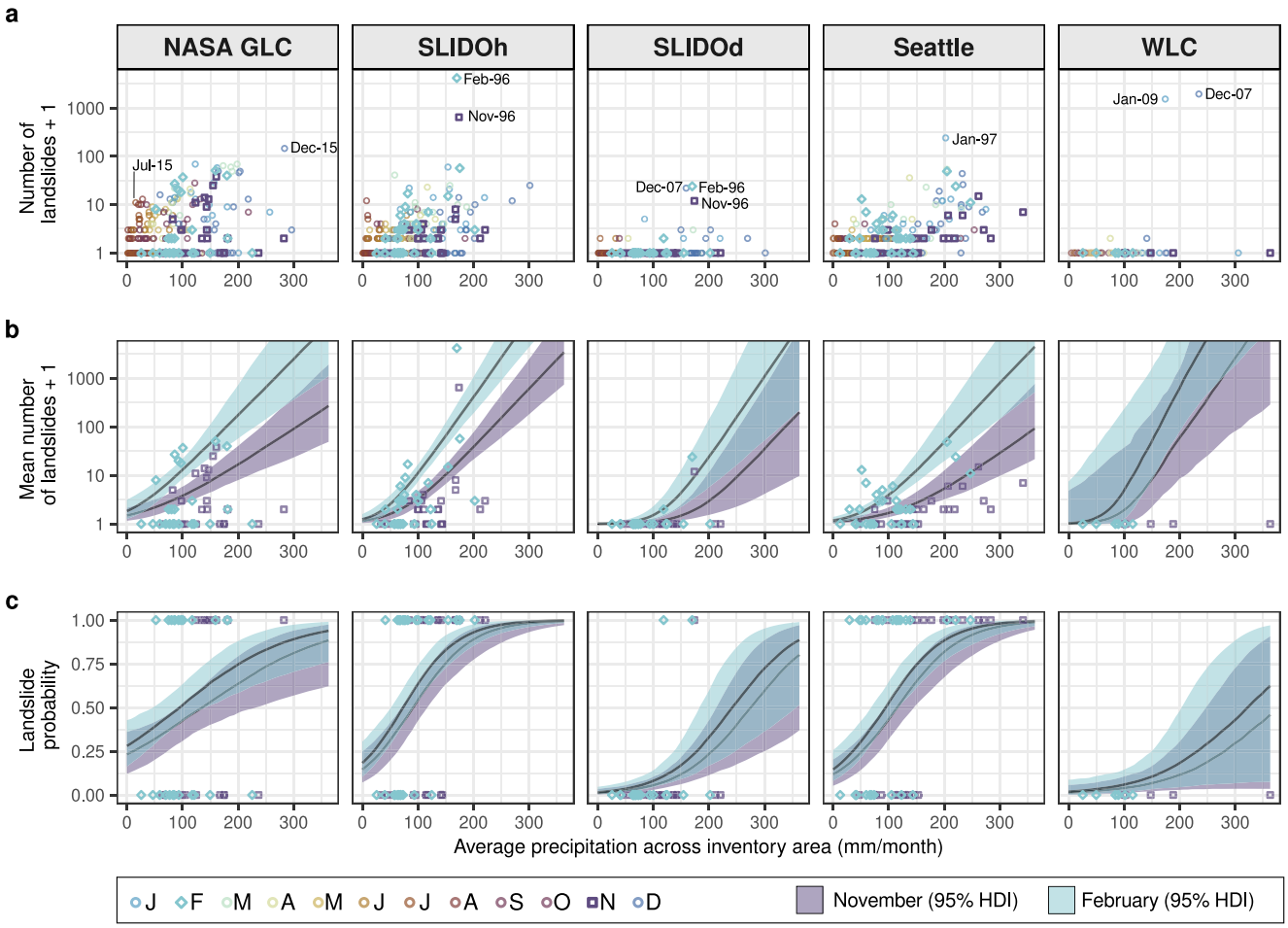

Figure 3. Monthly landslide response to precipitation from Bayesian regression. (a) Reported landslide count by month and inventory. Labeled points represent the highest counts reported in each inventory or months discussed in the text (month-year format). Posterior estimates of mean landslide (b) intensity, and (c) probability with average precipitation across inventory area for November and February.

Considering that median estimated counts are zero for all inventories between April and November, we also modeled the probability of any reported landslide in a given month. Our landslide-only multi-inventory logistic models show that landslides are most likely in January and become less so through June. The probability of landsliding is low, but non-zero, from June to October and increases again in November and December (Figure 2c). We observed credible differences between October and November and March and April in the Seattle and SLIDOh inventories. Landslide probabilities and their seasonal amplitude throughout the year are highest in the NASA inventory and lowest in WLC; again, we found that estimated variability between inventories is higher than between months (Figure S1 in Supporting Information S1).

Both landslide-only multi-inventory models reveal a seasonality in landslide activity that some single-inventory models are unable to show (NASA, SLIDOd, and WLC; gray symbols in Figure 2). The negative binomial multi-inventory model smooths the disjointed November and February landslide intensity peaks in the separate SLIDOh model, for example, and raises winter intensities for the NASA inventory, in each case informed by seasonal trends from the other inventories. Monthly uncertainties in the multi-inventory models are also well below those in single-inventory models, especially for catalogs containing mostly months without reported landslides (SLIDOd).

Comparing these results to 30-year normal monthly precipitation (PRISM Climate Group, 2021) over the areas covered by these inventories shows an offset between the annual precipitation pattern and landslide activity (Figure 2f). Mean monthly precipitation increased markedly from September to October, but landslide activity did not credibly increase until November. Similarly, precipitation in these areas peaked in November or Decem-

ber, whereas our results show that landslide probability peaked in January and intensity in February, lagging the annual peak in precipitation by one to two months.

Considering average precipitation as an additional predictor of both mean landslide intensity and probability shows a positive relationship between precipitation and both intensity and probability, regardless of month (Figure 3, Figures S3 and S4 in Supporting Information S1). However, across all precipitation values, landslide intensity is substantially elevated in February compared to November in all inventories (Figure 3); these differences are credible at the mean precipitation value for NASA GLC, SLIDOh, and Seattle (Figure S4 in Supporting Information S1). For example, in the NASA GLC, our model estimates an order of magnitude more landslides for 200-mm average precipitation in February than for the same amount in November (Figure 3b). Landslide probability, on the other hand, remains indistinguishable between months for a given precipitation average (Figure 3 and Figure S4 in Supporting Information S1). In all inventory areas, an average of 200 mm of precipitation would produce a similar estimated probability in both November and February; at monthly rainfall means above 200 mm, our models estimate that reported landslides are >95% probable in the SLIDOh and Seattle inventories.

5. Discussion and Conclusions

We investigated patterns of monthly landslide activity in the PNW with Bayesian multi-level models that unite data from five heterogeneous landslide inventories. Our multi-inventory models combine data from inventories with differing spatial and temporal coverage, data density, and reporting protocols to learn a regional seasonal pattern that some inventories show less distinctly and with higher uncertainties. Multi-inventory model results for monthly landslide intensity and probability both show a distinct seasonal pattern, with landslide activity peaking in winter, declining to a summer low, and increasing again in the fall. Credible increases in average monthly landslide intensity, inter-annual variability, and probability between October and November objectively mark the onset of the landslide season. Landslide intensity and probability increase with precipitation in all months, but landslide intensity is much higher for a given precipitation average at the peak of the landslide season in February compared to the onset in November (Figure 3).

This landslide seasonality in the PNW is largely linked to precipitation (Godt et al., 2006; Mirus, Morphew, & Smith, 2018), and most documented triggers or types in the inventories refer to rainfall-triggered shallow translational slides or flows. Heavy precipitation in the PNW mostly occurs between late October and mid-March, often linked to atmospheric rivers (Neiman et al., 2008, 2011) (Figure 2). Flooding in the PNW is also highly seasonal, with annual discharge peaks from November to January (Dougherty & Rasmussen, 2019; Neiman et al., 2011; Villarini, 2016). Our results expand previous conceptual models by showing that landslide seasonality lags the annual precipitation pattern by one to two months. The November landslide season onset follows the October precipitation increase; peak landslide probability in January and intensity in February come after November and December peaks in mean monthly precipitation. This lag indicates that landslide activity is highest when hillslopes have become sufficiently saturated, consistent with studies that have shown antecedent rainfall and resulting excess groundwater to be key predictors of landslide hazard on shorter, that is, hourly to daily timescales in the PNW (Godt et al., 2006; Mirus, Becker, et al., 2018; Scheevel et al., 2017).

Besides pointing to monthly lags, our models also show that a given amount of rain is expected to initiate far more landslides in February than in November (Figure 3), likely because slopes are primed for failure after having accumulated moisture over the winter (Godt et al., 2006). For example, in both February and November 1996, large storms triggered widespread shallow landslides and debris flows that are reported in the SLIDOh inventory (Burns et al., 1998; Harp et al., 1997) (Figure 3). Despite similar mean precipitation totals in those months, the February storm triggered over 4,000 reported landslides by delivering heavy rain to already wet, and in some areas snow-covered, hillslopes, whereas the November storm triggered a still disastrous 645 reported landslides. The February 1996 storm resulted in estimated direct damages of $100 million USD in Oregon alone (Wang et al., 2002). Unlike landslide intensity, landslide probability conditioned on precipitation remains comparable between all months, suggesting that while antecedent conditions are important for initiating many landslides, sufficient rain in any month is likely to initiate at least one landslide (Figure 3).

Our models also highlight that landslide counts are more variable in winter than in summer, when landslides are less probable. Nevertheless, summer landslide probability exceeds 25% in the NASA inventory. In July 2015, for example, 10 landslides were reported along roads or rivers in the NASA GLC; those with reported triggers were initiated by downpours, showing the effects of summer convective storms on the seasonal pattern of landsliding.

Overall, our multi-level modeling framework is able to learn more about regional landslide seasonality than models trained on individual inventories (Figure 2), but retains the data structure of all inventories. By design, a single seasonal pattern is learned from all of the inventories, but the amplitudes of monthly intensities or probabilities within that pattern differ by inventory. We find that the effects of inventory on landslide intensity exceed the effects of seasonality (Figure 2 and Figure S1 in Supporting Information S1); the resulting estimated number of landslides per area in Seattle is much higher than in the region covered by WLC, for example, Similarly, estimated landslide probability in January is 8% in the WLC inventory and 69% in the NASA inventory, despite the spatial overlap between these inventories. This apparent mismatch could arise from the physics of landslide occurrence or from the details of the recording protocol. Landslide activity in urban areas and along roads may be higher than in rural areas (Johnston et al., 2021), spatial variations in landslide susceptibility may be captured by different inventory footprints, or average landslide intensities may have differed in the time periods covered by the inventories (Lombardo et al., 2020). A more likely explanation is reporting bias arising from more detailed observations in urban areas and along roads (Steger et al., 2017). The monthly time-stamped landslides included in our study are a subset of all reported landslides: nearly all landslides reported in Seattle have a time-stamp, whereas only 8% of landslides reported in WLC have a time-stamp (Table S1 in Supporting Information S1). Ninety-nine percentage of dated landslides in WLC occurred on three unique days during major storms, whereas landslides in the Seattle inventory represent 823 days over 125 years (Table S1 in Supporting Information S1). Even if landslide activity in Seattle and the area covered by WLC were identical in space and time, a higher probability of recording landslides in Seattle would lead to higher apparent intensities and probabilities.

Given the different recording protocols between inventories, estimates from multi-inventory models (Figure 3) have additional advantages (Figure S2 in Supporting Information S1). Shrinkage refers to the difference between the single-inventory model parameter estimates and the multi-inventory model estimates and demonstrates how the inventories learn from each other (McElreath, 2020). The NASA inventory records landslides mostly along highways and in urban areas, and less so regional episodes that are recorded in WLC or SLIDOh. Parameter shrinkage pulls January and February intensity estimates up for the NASA inventory, as it learns about regional landslide episodes from the other inventories (green and gray points in Figure 2a). Conversely, the single-inventory estimates for SLIDOh are dominated by the regional storms in November and February 1996 (Figure 2 and Figure S2 in Supporting Information S1). Shrinkage pulls those estimates toward the global mean of the data, thus preventing overfitting. The same effect is observed when comparing the share of simulated months with landslides to the share of recorded months with landslides (Figure 3b and Figure S2 in Supporting Information S1). Single-inventory models tend to overfit the data, while the multi-inventory model generalizes better.

Altogether, our results show that Bayesian multi-level models are a useful and underexplored way to combine and reconcile information from multiple and seemingly incompatible landslide inventories. Potential further applications for combining inventory data or learning the variation between other groups are wide ranging: examples include intensity-duration thresholds for different seasons (Nikolopoulos et al., 2015; Peruccacci et al., 2012) or regions (Guzzetti et al., 2008), or combining multiple inventories in regression-based susceptibility models (Reichenbach et al., 2018).

Better understanding landslide activity at monthly to seasonal time-scales has the potential to improve emergency preparedness. Our results show that PNW landslide activity peaks in January–February, lagging mean monthly precipitation, and that similar rainfall leads to substantially higher intensities at the landslide season peak than at the onset. Because our models flexibly learn landslide activity by month from inventory data, they could be used to investigate landslide seasonality in regions with patterns as diverse as the winter-summer bimodal pattern observed in the western Himalaya and Karakoram (Hunt & Dimri, 2021), the East Asian Summer Monsoon peak in Japan (Saito et al., 2010), or the Atlantic hurricane season fall peak in Central America and the Caribbean (Sepúlveda & Petley, 2015). An important next step in seasonal landslide research will be to predict monthly intensity or probability for specific years, potentially considering global-interannual climate variability (Emberson et al., 2021), and eventually leading to operational forecasts. Such efforts will also pave the way for studies of whether and how climate change alters landslide seasonality.

Data Availability Statement

- NASA Global Landslide Catalog via https://data.nasa.gov/Earth-Science/Global-Landslide-Catalog/h9d8-neg4. Open Database License (NASA, 2018).

- Statewide Landslide Information Database for Oregon, release 4.2 (SLIDO-4.2) via https://www.oregongeology.org/pubs/dds/p-slido4.htm. Public (Franczyk et al., 2020).
- Seattle Historic Landslide Locations ECA: https://data-seattlecitygis.opendata.arcgis.com/datasets/6ac72973a5784d90bda0a5f8a001d9f3_22/explore?location=47.616250%2C-122.328600%2C11.91. PDDL License (City of Seattle, 2020).
- Washington Landslide Compilation: https://gis-qa.dnr.wa.gov/portal/home/item.html?id=da4255f770f84144b01c54010d533f4d. Public (Washington Geological Survey, 2020).
- PRISM 30-year climate normals 1991–2020 (Norm91m, v M3, Ppt, November 2021) are available at https://prism.oregonstate.edu/normals/. Monthly PRISM AN81m (v M3, Ppt, July 2015) precipitation data is available at https://ftp.prism.oregonstate.edu/monthly/ppt/ (PRISM Climate Group, 2021).
- Models were fit using brms version 2.17.0, available at https://cran.r-project.org/web/packages/brms/index.html (GPL-2) (Bürkner, 2017).
- The Python Jupyter and R Markdown Notebooks used for this analysis are available from Luna (2022) and can be found at https://github.com/lvluna/landslide-seasonality.

Acknowledgments
This research was funded by the DFG RTG "Natural Hazards and Risks in a Changing World" (NatRiskChange GRK 2043). We thank Natalie Lützow for help with data collection, Jürgen Kurths, and Norbert Marwan for feedback, and Ben Mirus and an anonymous reviewer for comments that helped to improve the manuscript. Open Access funding enabled and organized by Projekt DEAL.

References

Baum, R. L., & Godt, J. W. (2010). Early warning of rainfall-induced shallow landslides and debris flows in the USA. *Landslides*, *7*(3), 259–272. https://doi.org/10.1007/s10346-009-0177-0

Berti, M., Martina, M. L. V., Franceschini, S., Pignone, S., Simoni, A., & Pizziolo, M. (2012). Probabilistic rainfall thresholds for landslide occurrence using a Bayesian approach. *Journal of Geophysical Research*, *117*(F4). https://doi.org/10.1029/2012JF002367

Bürkner, P.-C. (2017). brms: An R package for Bayesian multilevel models using Stan. *Journal of Statistical Software*, *80*, 1–28. https://doi.org/10.18637/jss.v080.i01

Burns, S. F., Burns, W. J., James, D. H., & Hinkle, J. C. (1998). *Landslides in the Portland, Oregon metropolitan area resulting from the storm of February 1996: Inventory map, Database and evaluation* (p. 43). Portland State University. Retrieved from http://citeseerx.ist.psu.edu/viewdoc/download?doi=10.1.1.694.3602%26rep=rep1%26type=pdf

City of Seattle. (2020). *Historical landslide locations ECA*. City of Seattle. Retrieved from https://data-seattlecitygis.opendata.arcgis.com/datasets/6ac72973a5784d90bda0a5f8a001d9f3_22

Dougherty, E., & Rasmussen, K. L. (2019). Climatology of flood-producing storms and their associated rainfall characteristics in the United States. *Monthly Weather Review*, *147*(11), 3861–3877. https://doi.org/10.1175/MWR-D-19-0020.1

Emberson, R., Kirschbaum, D., & Stanley, T. (2021). Global connections between El Nino and landslide impacts. *Nature Communications*, *12*(1), 2262. https://doi.org/10.1038/s41467-021-22398-4

Franczyk, J. J., Burns, W. J., & Calhoun, N. C. (2020). *Statewide landslide information database for Oregon, release 4 (SLIDO-4.2)*. Oregon Department of Geology and Mineral Industries. Retrieved from https://www.oregongeology.org/pubs/dds/p-slido4.htm

Froude, M. J., & Petley, D. N. (2018). Global fatal landslide occurrence from 2004 to 2016. *Natural Hazards and Earth System Sciences*, *18*(8), 2161–2181. https://doi.org/10.5194/nhess-18-2161-2018

Gelman, A., & Hill, J. (2007). *Data analysis using regression and multilevel/hierarchical models*. Cambridge University Press.

Godt, J. W., Baum, R. L., & Chleborad, A. F. (2006). Rainfall characteristics for shallow landsliding in Seattle, Washington, USA. *Earth Surface Processes and Landforms*, *31*(1), 97–110. https://doi.org/10.1002/esp.1237

Guzzetti, F., Gariano, S. L., Peruccacci, S., Brunetti, M. T., Marchesini, I., Rossi, M., & Melillo, M. (2020). Geographical landslide early warning systems. *Earth-Science Reviews*, *200*, 102973. https://doi.org/10.1016/j.earscirev.2019.102973

Guzzetti, F., Peruccacci, S., Rossi, M., & Stark, C. P. (2008). The rainfall intensity–duration control of shallow landslides and debris flows: An update. *Landslides*, *5*(1), 3–17. https://doi.org/10.1007/s10346-007-0112-1

Harp, E. L., Chleborad, A. F., Schuster, R. L., Cannon, S. H., Reid, M. E., & Wilson, R. C. (1997). *Landslides and landslide hazards in Washington State due to February 5-9, 1996 storm*. U.S. Deptment of the Interior, U.S. Geological Survey. (p. 33). Retrieved from https://www.unisdr.org/preventionweb/files/1585_Washhrp.pdf

Hunt, K. M. R., & Dimri, A. P. (2021). Synoptic-scale precursors of landslides in the western Himalaya and Karakoram. *Science of the Total Environment*, *776*, 145895. https://doi.org/10.1016/j.scitotenv.2021.145895

Johnston, E. C., Davenport, F. V., Wang, L., Caers, J. K., Muthukrishnan, S., Burke, M., & Diffenbaugh, N. S. (2021). Quantifying the effect of precipitation on landslide hazard in urbanized and non-urbanized areas. *Geophysical Research Letters*, *48*(16), e2021GL094038. https://doi.org/10.1029/2021GL094038

Kirschbaum, D., Stanley, T., & Zhou, Y. (2015). Spatial and temporal analysis of a global landslide catalog. *Geomorphology*, *249*, 4–15. https://doi.org/10.1016/j.geomorph.2015.03.016

Korup, O. (2021). Bayesian geomorphology. *Earth Surface Processes and Landforms*, *46*(1), 151–172. https://doi.org/10.1002/esp.4995

Lewandowski, D., Kurowicka, D., & Joe, H. (2009). Generating random correlation matrices based on vines and extended onion method. *Journal of Multivariate Analysis*, *100*(9), 1989–2001. https://doi.org/10.1016/j.jmva.2009.04.008

Lombardo, L., Opitz, T., Ardizzone, F., Guzzetti, F., & Huser, R. (2020). Space-time landslide predictive modelling. *Earth-Science Reviews*, *209*, 103318. https://doi.org/10.1016/j.earscirev.2020.103318

Luna, L. V. (2022). Landslide-seasonality (Version 0.0.0). https://doi.org/10.5281/zenodo.6299024

McElreath, R. (2020). *Statistical rethinking: A Bayesian course with examples in R and STAN* (2nd ed.). Chapman and Hall/CRC Press.

Mirus, B. B., Becker, R. E., Baum, R. L., & Smith, J. B. (2018). Integrating real-time subsurface hydrologic monitoring with empirical rainfall thresholds to improve landslide early warning. *Landslides*, *15*(10), 1909–1919. https://doi.org/10.1007/s10346-018-0995-z

Mirus, B. B., Jones, E. S., Baum, R. L., Godt, J. W., Slaughter, S., Crawford, M. M., et al. (2020). Landslides across the USA: Occurrence, susceptibility, and data limitations. *Landslides*, *17*(10), 2271–2285. https://doi.org/10.1007/s10346-020-01424-4

Mirus, B. B., Morphew, M. D., & Smith, J. B. (2018). Developing hydro-meteorological thresholds for shallow landslide initiation and early warning. *Water*, *10*(9), 1274. https://doi.org/10.3390/w10091274

Napolitano, E., Fusco, F., Baum, R. L., Godt, J. W., & De Vita, P. (2016). Effect of antecedent-hydrological conditions on rainfall triggering of debris flows in ash-fall pyroclastic mantled slopes of Campania (southern Italy). *Landslides*, *13*(5), 967–983. https://doi.org/10.1007/s10346-015-0647-5

NASA. (2018). Global landslide catalog. NASA. Retrieved from https://data.nasa.gov/Earth-Science/Global-Landslide-Catalog/h9d8-neg4

Neiman, P. J., Ralph, F. M., Wick, G. A., Lundquist, J. D., & Dettinger, M. D. (2008). Meteorological characteristics and overland precipitation impacts of atmospheric rivers affecting the west coast of North America based on eight years of SSM/I satellite observations. *Journal of Hydrometeorology*, *9*(1), 22–47. https://doi.org/10.1175/2007JHM855.1

Neiman, P. J., Schick, L. J., Ralph, F. M., Hughes, M., & Wick, G. A. (2011). Flooding in western Washington: The connection to atmospheric rivers. *Journal of Hydrometeorology*, *12*(6), 1337–1358. https://doi.org/10.1175/2011JHM1358.1

Nikolopoulos, E. I., Borga, M., Marra, F., Crema, S., & Marchi, L. (2015). Debris flows in the eastern Italian Alps: Seasonality and atmospheric circulation patterns. *Natural Hazards and Earth System Sciences*, *15*(3), 647–656. https://doi.org/10.5194/nhess-15-647-2015

Nolde, N., & Joe, H. (2013). A Bayesian extreme value analysis of debris flows. *Water Resources Research*, *49*(10), 7009–7022. https://doi.org/10.1002/wrcr.20494

Peruccacci, S., Brunetti, M. T., Luciani, S., Vennari, C., & Guzzetti, F. (2012). Lithological and seasonal control on rainfall thresholds for the possible initiation of landslides in central Italy. *Geomorphology*, *139–140*, 79–90. https://doi.org/10.1016/j.geomorph.2011.10.005

Pollock, W., & Wartman, J. (2020). Human vulnerability to landslides. *GeoHealth*, *4*(10), e2020GH000287. https://doi.org/10.1029/2020GH000287

Pratt, C., Macciotta, R., & Hendry, M. (2019). Quantitative relationship between weather seasonality and rock fall occurrences north of Hope, BC, Canada. *Bulletin of Engineering Geology and the Environment*, *78*(5), 3239–3251. https://doi.org/10.1007/s10064-018-1358-7

PRISM Climate Group. (2021). *PRISM spatial climate datasets for the coterminous United States*. Oregon State University. Retrieved from https://prism.oregonstate.edu/

Reichenbach, P., Rossi, M., Malamud, B. D., Mihir, M., & Guzzetti, F. (2018). A review of statistically-based landslide susceptibility models. *Earth-Science Reviews*, *180*, 60–91. https://doi.org/10.1016/j.earscirev.2018.03.001

Saito, H., Nakayama, D., & Matsuyama, H. (2010). Relationship between the initiation of a shallow landslide and rainfall intensity—Duration thresholds in Japan. *Geomorphology*, *118*(1), 167–175. https://doi.org/10.1016/j.geomorph.2009.12.016

Scheevel, C. R., Baum, R. L., Mirus, B. B., & Smith, J. B. (2017). *Precipitation thresholds for landslide occurrence near Seattle, Mukilteo, and Everett, Washington*. (USGS Numbered Series No. 2017–1039) (p. 60). U.S. Geological Survey. https://doi.org/10.3133/ofr20171039

Schneuwly-Bollschweiler, M., & Stoffel, M. (2012). Hydrometeorological triggers of periglacial debris flows in the Zermatt valley (Switzerland) since 1864. *Journal of Geophysical Research*, *117*(F2), F02033. https://doi.org/10.1029/2011JF002262

Segoni, S., Piciullo, L., & Gariano, S. L. (2018). A review of the recent literature on rainfall thresholds for landslide occurrence. *Landslides*, *15*(8), 1483–1501. https://doi.org/10.1007/s10346-018-0966-4

Sepúlveda, S. A., & Petley, D. N. (2015). Regional trends and controlling factors of fatal landslides in Latin America and the Caribbean. *Natural Hazards and Earth System Sciences*, *15*(8), 1821–1833. https://doi.org/10.5194/nhess-15-1821-2015

Stan Development Team. (2022). Stan modeling language users guide and reference manual, version 2.28. Retrieved from https://mc-stan.org

Stanley, T. A., Kirschbaum, D. B., Benz, G., Emberson, R. A., Amatya, P. M., Medwedeff, W., & Clark, M. K. (2021). Data-driven landslide nowcasting at the global scale. *Frontiers of Earth Science*, *378*, 9. https://doi.org/10.3389/feart.2021.640043

Stanley, T. A., Kirschbaum, D. B., Sobieszczyk, S., Jasinski, M. F., Borak, J. S., & Slaughter, S. L. (2020). Building a landslide hazard indicator with machine learning and land surface models. *Environmental Modelling & Software*, *129*, 104692. https://doi.org/10.1016/j.envsoft.2020.104692

Steger, S., Brenning, A., Bell, R., & Glade, T. (2017). The influence of systematically incomplete shallow landslide inventories on statistical susceptibility models and suggestions for improvements. *Landslides*, *14*(5), 1767–1781. https://doi.org/10.1007/s10346-017-0820-0

Villarini, G. (2016). On the seasonality of flooding across the continental United States. *Advances in Water Resources*, *87*, 80–91. https://doi.org/10.1016/j.advwatres.2015.11.009

Wang, Y., Summers, R. D., & Hofmeister, R. J. (2002). *Landslide loss estimation pilot project in Oregon* (Open-File Report No. O-02-05). State of Oregon Department of Geology and Mineral Industries. Retrieved from https://oregonexplorer.info/data_files/OE_location/northcoast/documents/NorthCoastPDFs/O0205.pdf

Washington Geological Survey. (2020). Landslides compilation-GIS data, February 2020: Washington geological Survey digital data series 12, version 5.2. Retrieved from https://fortress.wa.gov/dnr/geologydata/publications/data_download/ger_portal_landslide_compilation.zip